Effect of fractal dimension of agglomerate structure on particle-particle interactions in turbulent flow

D.O. Njobuenwu and M. Fairweather

School of Chemical and Process Engineering, University of Leeds, Leeds LS2 9JT, UK d.o.njobuenwu@leeds.ac.uk; m.fairweather@leeds.ac.uk

Abstract – A systematic approach to simulate particle-particle interactions considering agglomerate breakup is developed using large eddy and discrete particle simulations, with the technique applied to solid-liquid flows in a vertical turbulent channel. The results indicate that the fractal dimension and size of the agglomerate are key parameters that control shear-induced breakup dynamics which becomes slower as the fractal dimension increases from $d_f = 2.0$ to $d_f = 3.0$, and ultimately to no breakup. Breakup processes reduce the number of agglomerates in the system as well as populating the system with particles of smaller size, thereby promoting more collisions and collisions leading to agglomeration. These results are encouraging and are consistent with expected physical behaviour.

1. Introduction

A fundamental understanding of particle-particle interactions (collision and agglomeration) and fluid-particle interactions (turbulence modulation, shear breakup) is essential for many environmental, biomedical, chemical and industrial applications. Examples include the nuclear industry which is where the motivation for this work comes from. The interest here is in the need to understand and control agglomeration in nuclear waste sludge transport and separation processes where high mass loadings are desirable to minimise waste volumes during waste processing. High particle concentrations result in particle-particle collisions, of which only a fraction lead to agglomeration, known as the collision efficiency.

Agglomeration is favoured when the cohesive force between particles is stronger than the kinetic energy between the colliding particles [1]. The individual agglomerates interact with the turbulent structures within a flow which may cause them to segregate into straining regions where they either breakup through the high shearing of the flow in these regions, or continue to grow with enhanced collision rates [2]. Agglomerates breakup when hydrodynamic stresses exceed a critical stress which characterises the agglomerate strength [3]. The rate of agglomeration and breakup in pumps and in pipe flow are important characteristics that feed into transport prediction models used in the nuclear industry [4]. Rector and Bunker [4], in studying how colloidal particles in sludge suspensions interact with each other, have shown that the primary particle size, agglomerate diameter and the fractal dimension of the agglomerate influence many of the key sludge properties, such as viscosity, sedimentation rate and sediment density. The general description of the multiscale interaction of the dispersed phase with a turbulent liquid flow is a challenging task due to inherent nonlinearities, inhomogeneities and coupling over disparate temporal and spatial scales [5-7].

One of the main computational fluid dynamic (CFD) tools being used to underpin the understanding of turbulent particle-laden two-phase flows is direct numerical simulation (DNS). Numerical complexity limits the DNS of turbulent multiphase flows

to small Reynolds number ($Re_\tau = 590$) e.g. [8, 9]. DNS of turbulent channel flow (single phase) up to $Re_\tau \approx 5200$ has appeared recently [10]. However, because of the presence of complex physical phenomena interacting with turbulence (multiphase flow, inter-particle collision, complex geometries) and the fact that the Reynolds number of industrial scale flows is generally orders of magnitude larger [7], the use DNS is not feasible. Recently, large eddy simulation (LES) has been adopted to study industrial and natural flow applications and for the study of complex-physics. LES with modelling of the sub-grid scale (SGS) motions and of their influence on particle dispersion can reproduce the results of DNS with reasonable accuracy and computational efficiency for turbulent particle-laden flow. Recently, Schutte et al. [11] have shown that the properties of the agglomerates change when two-way coupling is considered instead of one-way coupling, but not when LES is conducted instead of DNS. Schutte et al.'s [11] work shows that eddy resolving simulations (LES and DNS) can successfully capture particle-particle and particle-turbulence interactions.

Particles collide by different mechanisms and stick together forming irregular-shaped or fractal-like agglomerates. The structure of these agglomerates is characterised by the fractal dimension, d_f, and the pre-exponential factor, k_n, of simulated agglomerates of monodisperse primary particles for ballistic or diffusion-limited particle-agglomerate and agglomerate-agglomerate collision mechanisms [12]. Inci et al. [13] used Langevin dynamics to investigate the aggregation of soot nano-particles in turbulent flows, with the morphology of the aggregates characterised by the fractal dimension, d_f. A typical value of d_f for agglomerates formed by diffusion-limited agglomerate-agglomerate agglomeration is $d_f = 1.78$, while for diffusion-limited particle-agglomerate agglomeration $d_f = 2.5$, for ballistic agglomerate-agglomerate agglomeration $d_f = 1.90$, and for ballistic particle-agglomerate agglomeration $d_f = 3.0$, as reviewed by Eggersdorfer and Pratsinis [12]. The use of d_f to characterise agglomerates has become standard practice even though such particles may not fully obey fractal theory, but are sufficiently close to it to be called fractal-like. Therefore, our interest is in how the fractal dimension influences agglomerate breakup and, subsequently, particle collision and agglomeration processes.

In most numerical studies of the stability of colloidal suspensions, agglomeration is considered alone, without accounting for the breakup of agglomerates [7, 14-18]. The majority of the fundamental studies of particle agglomeration and breakup have been carried out under laminar flow conditions, for nano-sized particles and through the use of phenomenological approaches (e.g. population balance approach). In this paper, we investigate the competition between agglomeration and breakup using a previously well-validated LES [19] coupled to discrete particle simulation [7], an energy-balanced agglomeration model [14] and shear-induced agglomerate breakup [20]. We adopt in this work the shear-induced breakup of agglomerates model developed by Zaccone et al. [21] and Babler et al. [22]. This model has been implemented by Babler et al. [20] for estimation of the breakup rate of small aggregates in fully developed bounded and unbounded turbulence, and by Marchioli and Soldati [23] for the breakup of ductile agglomerates. This study is motivated as agglomeration and breakup define with time the morphology of the particles, and the transport and settling dynamics of the suspensions and sludges encountered in nuclear waste. The techniques proposed in this paper are fundamental and generic and can be applied to particle agglomeration and agglomerate breakup under similar

aerodynamic and hydrodynamic conditions to those that occur in various industrial and natural processes.

2. Mathematical Formulation

In LES, the fluid flow equations are spatially filtered, Eq. (1), so that the energy-containing large-scale turbulent motions are solved while the sub-grid scales are modelled:

$$\frac{\partial \bar{u}_i}{\partial x_i} = 0 \tag{1}$$

$$\frac{\partial \bar{u}_i}{\partial t} + \bar{u}_j \frac{\partial \bar{u}_i}{\partial x_j} = -\frac{1}{\rho}\frac{\partial \bar{p}}{\partial x_i} + \frac{\partial \bar{\tau}_{ij}}{\partial x_j} - \frac{\partial \tau_{ij}^{sgs}}{\partial x_j} + \frac{1}{\rho}\left(\bar{f}_i + \Pi\delta_{i3}\right) \tag{2}$$

The tensors $\bar{\tau}_{ij}$ and τ_{ij}^{sgs} are the viscous and the unknown SGS tensors, with the latter closed using the dynamically calibrated version of the Smagorinsky model [24, 25]. Coupling between the fluid and particle phases is incorporated by the addition of a momentum source, $\bar{f}_i$. The source term Π is the mean pressure gradient imposed that drives the flow and δ_{i3} is the Kronecker function ($\delta_{ij} = 1$ for $i = j$, $\delta_{ij} = 0$ for $i \neq j$). The mean pressure gradient, taking into account gravity and buoyancy forces, is given as [26, 27]:

$$\Pi = \frac{\Delta \bar{p}}{L_z} = -\frac{\rho u_\tau^2}{h} \pm \phi_v\left(\rho - \rho_p\right)g \tag{3}$$

where u_τ is the fluid shear velocity, ϕ_v is the particle volume fraction, h is the channel half-height, ρ_p is the particle density, g is acceleration due to gravity and the $\pm$ depends on the direction of gravity.

The motion of a particle in a turbulent flow is obtained from $\mathrm{d}\mathbf{x}_p = \mathbf{v}\mathrm{d}t$, with $\mathbf{v}$ given as:

$$\mathrm{d}\mathbf{v} = \left\{\frac{(\bar{\mathbf{u}} - \mathbf{v})}{\tau_p}f_D + C_{SL}\frac{3\rho}{4\rho_p}[(\bar{\mathbf{u}} - \mathbf{v}) \times \bar{\boldsymbol{\omega}}] + \frac{\rho}{\rho_p}\frac{\mathrm{D}\bar{\mathbf{u}}}{\mathrm{D}t} + \frac{\rho}{2\rho_p}\left(\frac{\mathrm{d}\bar{\mathbf{u}}}{\mathrm{d}t} - \frac{\mathrm{d}\mathbf{v}}{\mathrm{d}t}\right)\right\}\mathrm{d}t + \left(C_0\frac{k_{sgs}}{\tau_t}\right)^{0.5}\mathrm{d}\mathbf{W}_t \tag{4}$$

where the derivatives $\mathrm{d}/\mathrm{d}t = \partial/\partial t + \mathbf{v} \cdot \nabla\bar{\mathbf{u}}$ and $\mathrm{D}/\mathrm{D}t = \partial\bar{\mathbf{u}}/\partial t + \bar{\mathbf{u}} \cdot \nabla\bar{\mathbf{u}}$ represent Lagrangian derivatives, following the particle and the containing fluid element, respectively, and boldface symbols denote vector quantities. The terms in Eq. (4) are, respectively, contributions from the particle inertia, drag, shear lift, pressure-gradient, and added-mass forces, and a stochastic force term accounting for the influence of the SGS fluid velocity fluctuations on particle acceleration [19]. $\mathbf{v}$ and $\mathbf{x}_p$ are the particle instantaneous velocity and position; $\bar{\mathbf{u}}$ and $\bar{\boldsymbol{\omega}} = 0.5(\nabla \times \bar{\mathbf{u}})$ are known resolved fluid velocities and rotation interpolated at particle position. The terms f_D and C_{SL} are, respectively, the drag and shear lift forces terms taken from the Schiller and Naumann drag correlation [28] and the Mei [29] shear lift force correlation, both due to the particles' finite Reynolds number.

For the stochastic term, $C_0 = 1$ is a dispersion coefficient [19] and the unresolved kinetic energy $k_{sgs} = 2\Delta^2 C_S^{2/3} \bar{S}_{ij}\bar{S}_{ij}$ of the continuous phase is computed assuming equilibrium of the small scales. The term $d\mathbf{W}_t = \boldsymbol{\xi} \times \sqrt{dt}$ is the incremental Wiener term, where $\boldsymbol{\xi}$ is a random vector sampled with zero mean and a variance of unity, independently for each time step. The parameters Δ, C_S and $\bar{S}_{ij}$ are the filter width, Smagorinsky constant and filtered strain tensor. The interaction between particles and fluid phase turbulence is considered by the time scale, $\tau_t = \tau_p$. Other alternative time scales are reported in Bini and Jones [19].

Particle-particle interaction is modelled using the deterministic hard sphere collision model due to binary collisions and neglecting particle angular momentum. The concept of virtual cells [30] is adopted. The computational domain is decomposed into $d_x \times d_y \times d_z$ virtual cells. The standard deterministic collision detection procedure is limited to the particles in each virtual cell. The use of the concept of virtual cells enables the cost of checking for collisions to be reduced from $O(N_0^2)$, when collisions between all possible particle pairs are considered, to $O(N_0)$.

In order that two particles within a virtual cell collide, two conditions have to be fulfilled [31]. The first condition is that they must approach each other, expressed as $(\mathbf{x_r} \cdot \mathbf{v_r} < 0)$, where $\mathbf{x_r}$ and $\mathbf{v_r}$ are the relative separation distance and the relative velocity between the two particles, respectively. The second condition is that the minimum separation distance, $\mathbf{x_{r,min}}$ occurring at Δt_{min} within a time step Δt, must be less than the sum of the particles' radii, $d_{12} = (d_{p,1} + d_{p,2})/2$. Therefore contacts between neighbouring particles within a time step are detected by satisfying the conditions [31]:

$$(\mathbf{x_r} \cdot \mathbf{v_r} < 0) \ \& \ \left(\left|\mathbf{x_{r,min}}\right| \leq d_{12}\right) \ \& \ (\Delta t_{min} \leq \Delta t) \tag{5}$$

If a collision is detected, the position and velocity vectors of the colliding particles are updated as per the hard-sphere model [30, 31].

Agglomeration for the colliding particles is based on an extension of the hard-sphere collision expression in which agglomeration is permitted if the elastic energy (i.e. the relative kinetic energy before the collision minus the dissipated energy) after the compression period of the collision is less than the work required to overcome the van der Waals forces [1]:

$$\frac{(\mathbf{v}_2^- - \mathbf{v}_1^-)^2 - [(\mathbf{v}_2^- - \mathbf{v}_1^-) \cdot \mathbf{n_c}]^2(1 - e_n^2)}{|(\mathbf{v}_2^- - \mathbf{v}_1^-) \cdot \mathbf{n_c}|} \leq \frac{H^*}{6\delta_0^{*2}} \left[(1 - e_n^2)\frac{6}{\pi^2 \rho_p^* \bar{p}^*}\frac{d_{p,1}^{*3} + d_{p,2}^{*3}}{d_{p,1}^{*2} d_{p,2}^{*2}(d_{p,1}^* + d_{p,2}^*)}\right]^{1/2} \tag{6}$$

where quantities with the superscript * are made dimensionless in the integral scale using the channel half-height, h, the bulk velocity, u_b, and the fluid density, ρ. The agglomerate size and structure are based on a volume-equivalent sphere.

Breakup is assumed to occur when the local hydrodynamic stress $\sigma \sim \mu(\epsilon/\nu)^{1/2}$ at the agglomerate position, acting on the agglomerate, exceeds a critical stress, σ_{cr} [20]:

$$\sigma_{cr} \sim r^{-q} = N_{pp}^{-q/d_f} \tag{7}$$

where $N_{pp} \sim r^{d_f}$ is the number of primary particles constituting the agglomerate, d_f is the agglomerate fractal dimension, r is the radius of the primary particle, and $q = [9.2(3 - d_f) + 1]/2$ is a scaling exponent that depends on the agglomerate structure [20]. On detecting breakup, the agglomerate is broken into two parts, a frequently used modelling assumption made mainly because of the lack of data on other types of breakup modes.

3. Numerical Solution

The set of equations (Eqs. (1) and (2)) was discretised onto a co-located grid arrangement. The numerical computations were carried out with a parallelised (by domain decomposition) second-order accurate finite-volume code called BOFFIN (boundary fitted flow integrator) [32]. It is based on a fully implicit low-Mach-number formulation and is second-order accurate in space and time. For the momentum equation convection terms, an energy-conserving discretisation scheme is used and all other spatial derivatives are approximated by standard second-order central differences. Time derivatives are approximated by a three-point backward difference scheme with variable time step to ensure that the maximum Courant number, based on the filtered velocity, always lies between 0.1 and 0.2. A two-step, second-order, time-accurate approximate factorisation method is applied to determine the pressure and ensure mass conservation in conjunction with a pressure smoothing technique to prevent even-odd node uncoupling of the pressure and velocity fields. The system of algebraic equations resulting from the discretisation is solved using the matrix preconditioned conjugate gradient method BI-CGSTAB for the matrix of velocity vectors, and ICCG for the pressure.

The channel flow used for the simulations has the configuration: coordinates $(x \times y \times z)$, computational domain size $(2h \times \pi h \times 2\pi h)$ and grid nodes $(129 \times 128 \times 128)$ in the wall-normal, spanwise and streamwise directions, respectively. The shear Reynolds number $Re_\tau = h u_\tau / v$ is 590, with $h = 0.02\,m$, kinematic viscosity $v = 1.0 \times 10^{-6}\,m^2 s$ and $\rho = 1000\,kg\,m^3$. The mesh spacing is uniform in the y and z directions but stretched in the x direction by a hyperbolic stretching function. The non-dimensional values of parameters associated with length, velocity and time scales are presented in wall units $(^+)$ following normalisation with u_τ and v. Periodic boundary conditions are used in the streamwise and spanwise directions. In the streamwise direction, the mean pressure gradient, Π in Eq. (3), is imposed as a source term to drive the flow. Other details of the numerical, initial and boundary conditions can be found elsewhere [7].

The channel was laden with spherical calcite particles, a simulant for legacy waste sludge, with the properties: diameter $d_p = 60\,\mu m$, density $\rho_p = 2170\,kg$, volume fraction $\phi_v \sim O(10^{-3})$, Hamaker constant $H = 3.8 \times 10^{-20}\,J$, mean yield stress $\bar{\sigma} = 3.0 \times 10^8\,Pa$, minimal contact distance $\delta_0 = 2.0 \times 10^{-10}\,m$ and normal restitution coefficient $e_n = 0.4$. The particle equation of motion was integrated using a fourth-order Runge-Kutta scheme following interpolation of the fluid properties at the particle position, with elastic collisions applied at the walls [7].

4. Results and Discussion

The computed statistics of the mean streamwise velocity, $\langle u_z^+ \rangle$, of the root mean

square values of the velocity fluctuations along the wall-normal, $\langle u_x'^+ \rangle$, spanwise, $\langle u_y'^+ \rangle$, and streamwise, $\langle u_z'^+ \rangle$, directions, and of the $x - z$ component of the Reynolds shear stress, $\langle u_x'^+ u_z'^+ \rangle$ are shown in Figure 1. Note that the statistics presented here were gathered from resolved velocities over $10H/u_\tau$ containing samples taken after each time step ($\Delta t = 3.5 \times 10^{-4}$ s). The results are time- and space-averaged (denoted by $\langle \cdots \rangle$) as well as averaged over the two halves of the channel, to increase the reliability of the statistical sample. These statistical moments from the present LES are compared with DNS results for turbulent channel flow at $Re_\tau = 590$ [33]. The comparisons show very good agreement, confirming that the use of a highly resolved LES and dynamic modelling of the SGS term gives reliable results.
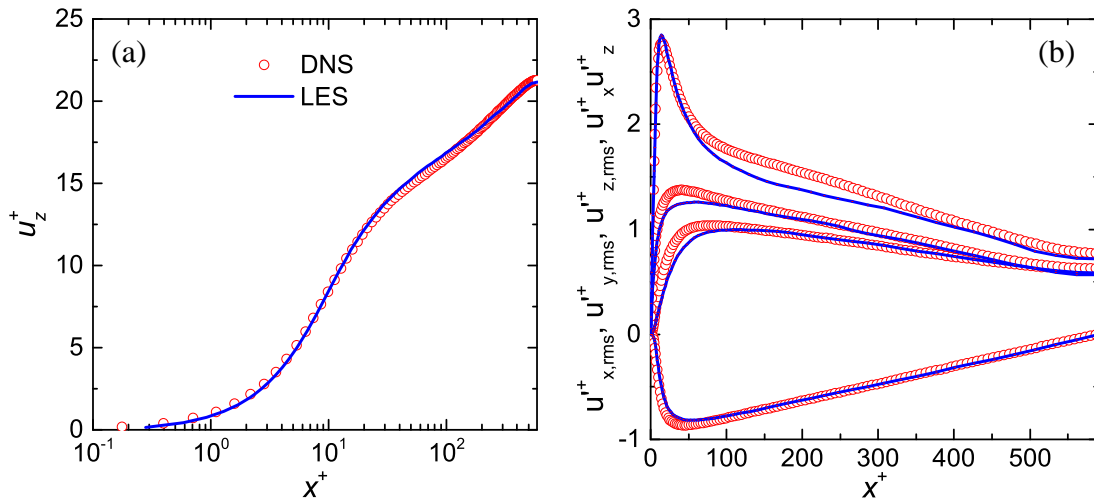

Figure 1: Statistics of (a) the mean streamwise velocity, $\langle u_z^+ \rangle$, and (b) the root mean square of the velocity fluctuations along the wall-normal, $\langle u_x'^+ \rangle$, spanwise, $\langle u_y'^+ \rangle$, and streamwise, $\langle u_z'^+ \rangle$, directions, and the Reynolds shear stress, $\langle u_x'^+ u_z'^+ \rangle$, for turbulent channel flow simulations at shear Reynolds number $Re_\tau = 590$.

The agglomeration kinetics, as illustrated in Figure 2(a), are such that during the agglomeration process, two primary particles (monomers, $N_{a,i=1}$) collide and agglomerate to form a dimer, $N_{a,i=2}$, while a monomer and a dimer collide to form a trimer, $N_{a,i=3}$, which is an agglomerate of three primary particles, and so on. The breakup kinetics, as illustrated in Figure 2(b), are the direct opposite to that of agglomeration, such that a trimer breaks up into a monomer and a dimer and so on.
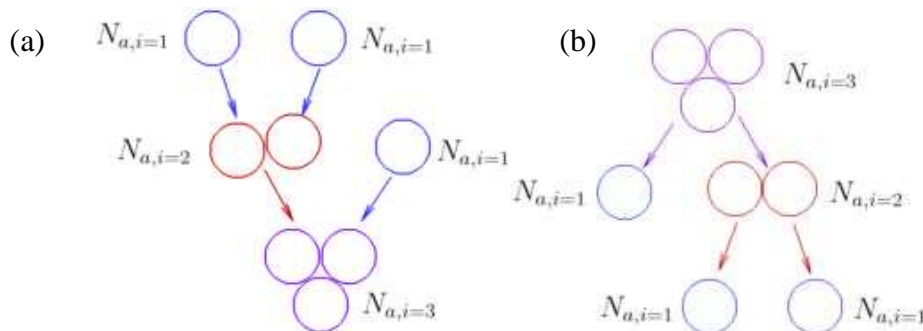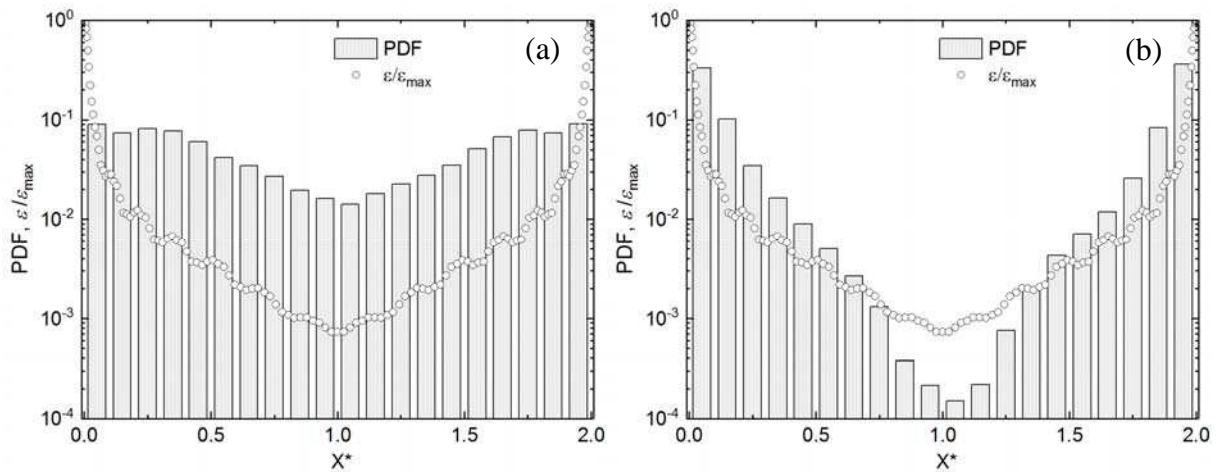

Figure 2: Schematic of (a) particle agglomeration process and (b) agglomerate breakup process.

To examine the extent to which the agglomerate fractal dimension, d_f, during agglomerate breakup processes influences the global agglomeration process as well as the transient and the steady-state behaviour of the system, a series of simulations were carried out. The value of the agglomerate fractal dimension, d_f, was set to 2.0, 2.5, 2.8 and 3.0. An additional fifth simulation, as a control, was the case of no breakup for which $d_f \to \infty$. The effect of the fractal dimension on the locations where breakup events occur, irrespective of the agglomerate type (or size) involved, is shown in the probability density function, $PDF(x^*)$, in Figure 3. The time- and spaced-averaged turbulence kinetic energy dissipation rate, ϵ, normalised by its maximum value ϵ_{max}, is also shown in Figure 3. The turbulence energy dissipation rate determines the intensity of the turbulence shear gradient, turbulent length and time scales. The turbulence kinetic energy and its dissipation rate have a distinct influence on the particle transport, agglomeration and breakup process. As seen in Figure 3, the turbulent kinetic breakup is greatest in the near-wall regions. Hence, the hydrodynamic stresses, $\sigma \sim \epsilon^{1/2}$, resulting from the local energy dissipation rate, ϵ, are largest in the near-wall regions of the channel. In conjunction with ϵ, it is evident in Figure 3 that the fractal dimension has a large effect on the probability of the location along the wall-normal direction, x^*, where agglomerate breakup occurs. For fractal dimension $d_f = 2.0$, Figure 3(a) shows agglomerate breakup occurring at all positions between the two parallel walls bounding the channel flow. Most of the breakup presented in Figure 3(a) occurred in the near-wall regions. This observation is significantly different when compared to all other cases with $d_f > 2.0$. Regarding the agglomerate critical stress, σ_{cr}, which characterises agglomerate strength, the agglomerate strength is strongly dependent on d_f, hence, breakup occurs mostly in the near-wall regions where the local hydrodynamic stress, $\sigma \sim \epsilon^{1/2}$, resulting from the local turbulence kinetic energy dissipation rate, ϵ, is largest. For the $d_f = 2.8$ and 3.0 cases, agglomerate breakup occurs at the plane closest to the walls where the stresses are at a maximum value.
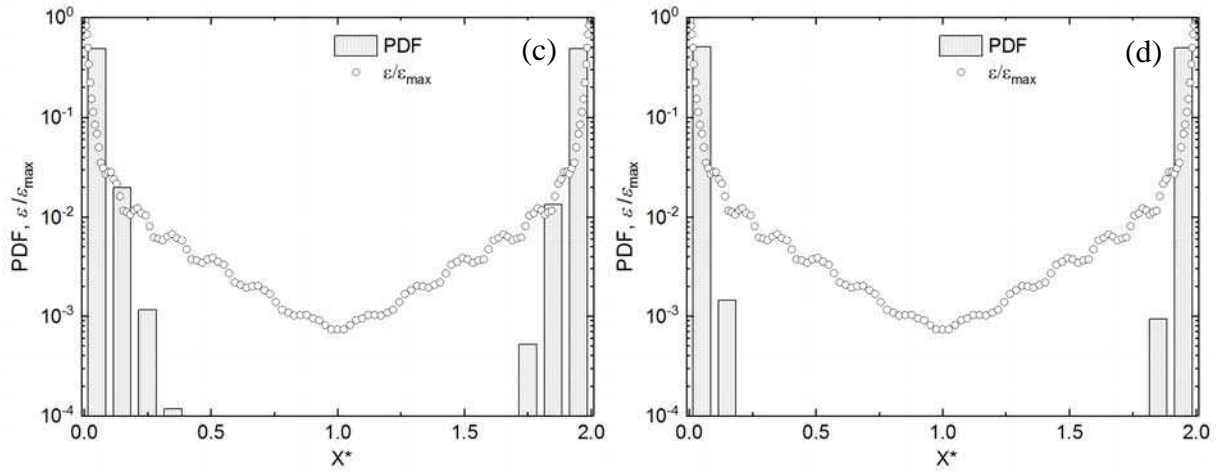
Figure 3: Effect of fractal dimension of the agglomerate structure, d_f, on the probability density function, $PDF(x^*)$, of the non-dimensional position in the wall-normal direction where agglomerate breakup occurs: (a) $d_f = 2.0$, (b) 2.5, (c) 2.8 and (d) 3.0. The graph of the mean fluid un-laden dissipation rate, ϵ, normalised by the maximum dissipation rate, ϵ_{max}, with respect to $x^* = x/h$ is superimposed.

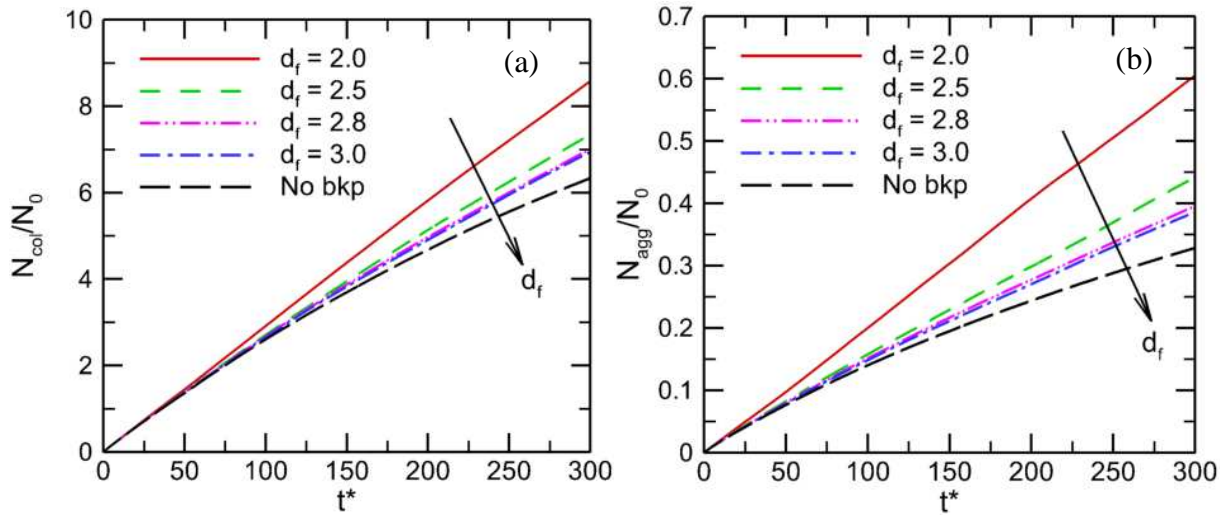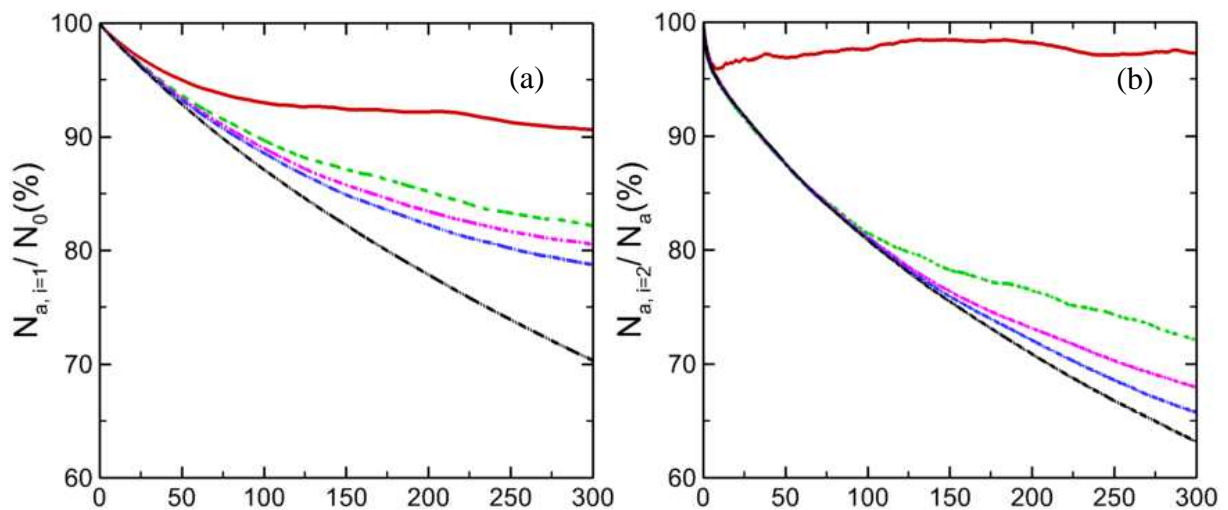

Figure 4: Influence of fractal dimension d_f of the agglomerate structure on the time ($t^* = tu_b/h$) history of (a) the total number of collision, N_{col}, normalised by the initial number of primary particles, N_0 and (b) the total number of the particle-particle collisions leading to agglomeration, N_{agg}, normalised by the initial number of primary particles.

Figure 4(a) shows the influence of the fractal dimension of the agglomerate structure on the total number of accumulated particle-particle collisions, N_{col}, normalised by the initial number of primary particles injected, N_0, as a function of time. Similarly, Figure 4(b) shows the temporal development of the population of inter-particle collisions leading to agglomeration, N_{agg}/N_0, hereafter called agglomeration events, for four values of the fractal dimension, $d_f = 2.0, 2.5, 2.8, 3.0$ and for the case of no breakup (*No bkp*). Figure 4(a) shows that the breakup model with $d_f = 2.0$ predicts the greatest number of particle-particle collisions, consistent with the breakup events mentioned in Figure 3. More collisions occur with decreasing fractal dimension from the limiting case of no-breakup through $d_f = 3.0$ to $d_f = 2.0$. It

is obvious that the breaking of an agglomerate in the system populates the system with particles with a smaller number of primary particles which have a higher propensity to collision and subsequent agglomeration [7, 14, 34]. Hence, as more breakup occurs with time, its effect on the number of collision in Figure 4(a) is more pronounced than at earlier simulation times. Similarly, the agglomeration events, N_{agg}/N_0, in Figure 4(b) decrease as the breakup events are increased from no breakup through $d_f = 3.0$ to $d_f = 2.0$. The case with $d_f = 2.0$ has the highest number of agglomeration events consistent with the largest number of inter-particle collisions, as well as the highest number of breakup events. The large number of inter-particle collisions is a prerequisite for a large number of agglomeration processes, assuming that the sticking force is great enough [14], while breakup events populate agglomerates with fewer numbers of primary particles, a precursor to a high collision rate [7, 18].

The transient particle size distributions, in which the primary particles (single (1), $N_{a,i=1}$) are presented as a percentage of the initial number of all primary particles, N_0, and the agglomerates (double (2), triple (3), etc, $N_{a,i>1}$) are presented as a percentage of the total number of all agglomerates N_a, at time t^* are given in Figure 5 for all breakup cases considered. For the single particles, the profiles start at 100% when the system is populated by only the $N_{a,i=1}$ sized particles. As time progresses and pair-formation and cluster-cluster formation phases set in, more $N_{a,i=1}$ particles are consumed leading to an immediate reduction in their number. However, as the system progresses further into the breakup phase, the population balance of the $N_{a,i=1}$ sized single particles predicted by the $d_f = 2.0$ case starts increasing with time until the profile flattens out at a steady level of about 90%. At this point, there appears to be an equilibrium between the rate of consumption of $N_{a,i=1}$ sized particles producing agglomerates, and the rate of their replenishment due to the breakup of agglomerates. Contrary to the behaviour of the $d_f = 2.0$ case, the other cases continue to reduce with time, with the reduction rate inversely proportional to the strength of the agglomerate, and with the base case of no breakup showing about 70% of $N_{a,i=1}$ particles remaining at $t^* = 300$.
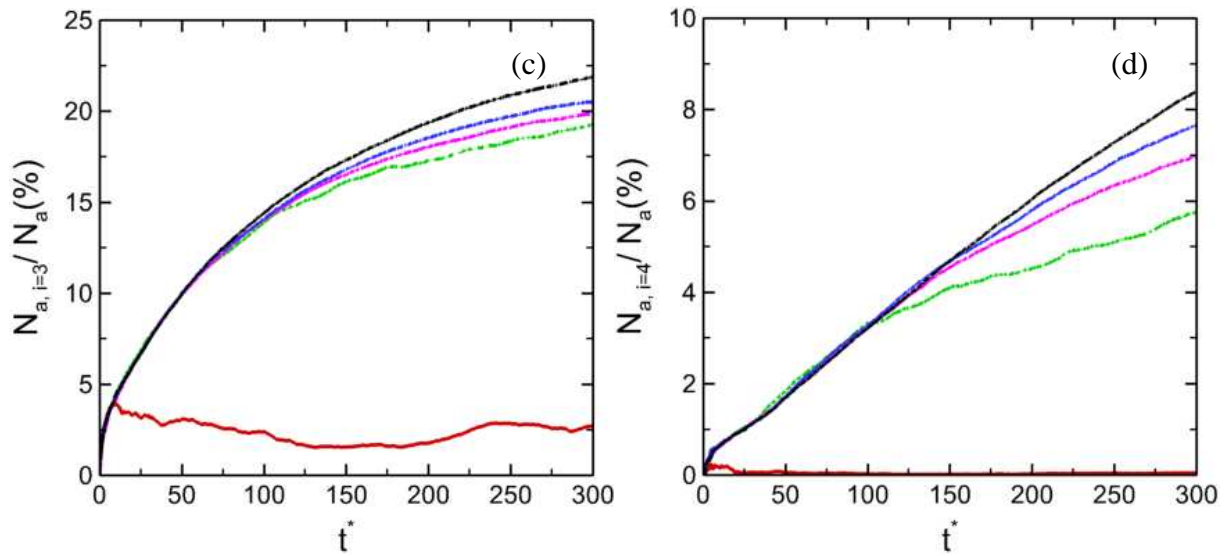
Figure 5: Influence of fractal dimension, d_f, of the agglomerate structure on the time history of the particle size distribution, $N_{a,i}$, expressed as (a) the percentage of the evolution of the primary particle size, $N_{a,i=1}$, normalised by the initial number of primary particle, N_0, and (b, c, d), expressed as the percentage of the population of the agglomerate size, $N_{a,i>1}$, normalised by the total number of agglomerates present, N_a (Colours: red, $d_f = 2.0$; green, $d_f = 2.5$; magenta, $d_f = 2.8$, blue, $d_f = 3.0$ and black, *No bkp*).

For the population balance of the agglomerates, $N_{a,i \geq 2}$, shown in Figure 5, it follows that the rate of consumption of the double, triple and quadruple particles in the production of larger sized agglomerates, and the rate of replenishment of that agglomerate type due to breakup, is identical for the weakest agglomerate structure case ($d_f = 2.0$). The percentage of the agglomerate for $d_f = 2.0$ stabilises at about 95%, 2.5% and 0% for the $N_{a,i=2}$, $N_{a,i=3}$ and $N_{a,i=4}$ cases, respectively. However, for the $d_f > 2.0$ cases, the relationship between the rate of production of the agglomerate sizes and their corresponding consumption varies depending on the agglomerate size. In the case of the double sized agglomerates, $N_{a,i=2}$, their population reduces with time, with no significant breakup occurring and their number being depleted with time due to agglomeration only. For the larger agglomerate sizes, $N_{a,i=3}$ and $N_{a,i=4}$, their number increases with time such that their population is skewed towards their production rather than towards depletion by either breakup or agglomeration.

4. Conclusions

Large eddy simulation and discrete particle simulation have been used to simulate particle-particle interactions (inter-particle collisions and agglomeration) and breakup processes, together with a deterministic treatment of inter-particle collisions and particle feedback effects on the fluid phase (though not shown). Agglomeration is based on the pre-collision energy-momentum balance, restitution coefficient and van der Waals interactions. To allow the CFD tool to ultimately be applied to practical processes, the BOFFIN LES code was extended to handle the breakup of agglomerates. Agglomerate breakup occurs instantaneously subject to the hydrodynamic stress exceeding a critical value dictated by the properties of the

agglomerates. The expression for the critical stress to be overcome to allow breakup indicates that the fractal dimension and size of the agglomerate are key parameters that control breakup process. The results show that the fragmentation dynamics of an agglomerate become slower as the fractal dimension increases. Breakup events also increase with time as larger agglomerates, which are weaker in strength and more susceptible to breakup, are formed. Breakup events therefore reduce the number of agglomerates in the system as well as populating the system with particles of smaller size, thereby promoting more collisions and collisions leading to agglomeration. The base case of no breakup followed the behaviour previously reported in the literature [7, 14, 15, 18, 34].

These results support the conclusion that the local kinetic energy dissipation rate controls the kinetics of the agglomerate breakup process, while the kinetic energy controls the collision agglomeration processes which occurs mostly in the bulk region of the channel. The bulk flow helps in transporting the agglomerates towards the high shear stress zones where the agglomerates experience high dissipation rates and break when these stresses overcome the threshold that characterises the strength of the agglomerate.

The techniques developed and implemented here provide a powerful tool for the simulation of particle-laden flows, and for predicting their evolution with time under turbulent flow conditions. Finally, it should be mentioned that further validation of the techniques reported here requires detailed experimental data which, at the present time, are scarce.

Acknowledgements

References

1. M. Breuer and N. Almohammed. Modeling and simulation of particle agglomeration in turbulent flows using a hard-sphere model with deterministic collision detection and enhanced structure models. *Int. J. Multiphase Flow*, 73: 171-206, 2015.
2. G. Falkovich, A. Fouxon and M.G. Stepanov. Acceleration of rain initiation by cloud turbulence. *Nature*, 419: 151-154, 2002.
3. R. Wengeler and H. Nirschl. Turbulent hydrodynamic stress induced dispersion and fragmentation of nanoscale agglomerates. *J. Colloid Interface Sci.*, 306: 262-273, 2007.
4. D.R. Rector and B.C. Bunker. Effect of colloidal aggregation on the sedimentation and rheological properties of tank waste. Pacific Northwest National Laboratory, PNL-10761, Richland, USA, 1995.
5. B. Rosa and L.-P. Wang. Parallel implementation of particle tracking and collision in a turbulent flow. In *Parallel Processing and Applied Mathematics: Eight International Conference (Edited by R. Wyrzykowski, J. Dongarra, K. Karczewski and J. Wasniewski)*, pp. 388-397, Springer, 2010.
6. C. Henry, J.-P. Minier and G. Lefèvre. Towards a description of particulate fouling: From single particle deposition to clogging. *Adv. Colloid Interface Sci.*, 185-186:

34-76, 2012.

7. D.O. Njobuenwu and M. Fairweather. Simulation of deterministic energy-balance particle agglomeration in turbulent liquid-solid flows. *Phys. Fluids*, 29: 083301, 2017.

8. L. Zhao, C. Marchioli and H.I. Andersson. Slip velocity of rigid fibers in turbulent channel flow. *Phys. Fluids*, 26: 063302 2014.

9. S. Sundaram and L.R. Collins. Collision statistics in an isotropic particle-laden turbulent suspension. Part 1. Direct numerical simulations. *J. Fluid Mech.*, 335: 75-109, 1997.

10. M. Lee and R.D. Moser. Direct numerical simulation of turbulent channel flow up to $Re_t \sim 5200$. *J. Fluid Mech.*, 774: 395-415, 2015.

11. K.C.J. Schutte, L.M. Portela, A. Twerda and R.A.W.M. Henkes. Hydrodynamic perspective on asphaltene agglomeration and deposition. *Energy Fuels*, 29: 2754-2767, 2015.

12. M.L. Eggersdorfer and S.E. Pratsinis. The structure of agglomerates consisting of polydisperse particles. *Aerosol Sci. Technol.*, 46: 347-353, 2012.

13. G. Inci, A. Kronenburg, R. Weeber and D. Pflüger. Langevin dynamics simulation of transport and aggregation of soot nano-particles in turbulent flows. *Flow Turbul. Combust.*, 98: 1065-1085, 2017.

14. M. Breuer and N. Almohammed. Modeling and simulation of particle agglomeration in turbulent flows using a hard-sphere model with deterministic collision detection and enhanced structure models. *Int. J. Multiphase Flow*, 73: 171-206, 2015.

15. N. Almohammed and M. Breuer. Modeling and simulation of agglomeration in turbulent particle-laden flows: A comparison between energy-based and momentum-based agglomeration models. *Powder Technol.*, 294: 373-402, 2016.

16. M. Afkhami, A. Hassanpour, M. Fairweather and D.O. Njobuenwu. Fully coupled LES-DEM of particle interaction and agglomeration in a turbulent channel flow. *Comput. Chem. Eng.*, 78: 24-38, 2015.

17. A.S. Hellestø, M. Ghaffari, B.V. Balakin and A.C. Hoffmann. A parametric study of cohesive particle agglomeration in a shear flow - Numerical simulations by the discrete element method. *J. Dispersion Sci. Technol.*, 38: 611-620, 2017.

18. D.O. Njobuenwu and M. Fairweather. Deterministic modelling of particle agglomeration in turbulent flow. In *Eighth International Symposium on Turbulence, Heat and Mass Transfer (Edited by K. Hanjalic, T. Miyauchi, D. Borello, M. Hadziabdic and P. Venturini)*, pp. 587-590, 2015.

19. M. Bini and W. Jones. Particle acceleration in turbulent flows: A class of nonlinear stochastic models for intermittency. *Phys. Fluids*, 19: 035104, 2007.

20. M.U. Babler, L. Biferale, L. Brandt, U. Feudel, K. Guseva, A.S. Lanotte, C. Marchioli, F. Picano, G. Sardina, A. Soldati and F. Toschi. Numerical simulations of aggregate breakup in bounded and unbounded turbulent flows. *J. Fluid Mech.*, 766: 104-128, 2015.

21. A. Zaccone, M. Soos, M. Lattuada, H. Wu, M.U. Bäbler and M. Morbidelli. Breakup of dense colloidal aggregates under hydrodynamic stresses. *Phys. Rev. E*, 79: 061401, 2009.

22. M.U. Babler, L. Biferale and A.S. Lanotte. Breakup of small aggregates driven by turbulent hydrodynamical stress. *Phys. Rev. E*, 85: 025301, 2012.

23. C. Marchioli and A. Soldati. Turbulent breakage of ductile aggregates. *Phys. Rev. E*, 91: 053003, 2015.

24. M. Germano, U. Piomelli, P. Moin and W.H. Cabot. A dynamic subgrid-scale eddy viscosity model. *Phys. Fluids*, 3: 1760-1765, 1991.
25. U. Piomelli and J. Liu. Large-eddy simulation of rotating channel flows using a localized dynamic model. *Phys. Fluids*, 7: 839-848, 1995.
26. Y. Yamamoto, M. Potthoff, T. Tanaka, T. Kajishima and Y. Tsuji. Large-eddy simulation of turbulent gas–particle flow in a vertical channel: effect of considering inter-particle collisions. *J. Fluid Mech.*, 442: 303-334, 2001.
27. D. Molin, C. Marchioli and A. Soldati. Turbulence modulation and microbubble dynamics in vertical channel flow. *Int. J. Multiphase Flow*, 42: 80-95, 2012.
28. R. Clift, J.R. Grace and M.E. Weber, Bubbles, drops and particles*,* Academic Press, 1978.
29. R. Mei. An approximate expression for the shear lift force on a spherical particle at finite reynolds number. *Int. J. Multiphase Flow*, 18: 145-147, 1992.
30. M. Breuer and M. Alletto. Efficient simulation of particle-laden turbulent flows with high mass loadings using LES. *Int. J. Heat Fluid Flow*, 35: 2-12, 2012.
31. M. Chen, K. Kontomaris and J.B. McLaughlin. Direct numerical simulation of droplet collisions in a turbulent channel flow. Part I: Collision algorithm. *Int. J. Multiphase Flow*, 24: 1079-1103, 1999.
32. W.P. Jones, F. di Mare and A.J. Marquis, LES-BOFFIN: Users guide, technical memorandum, Mechanical Engineering Department, Imperial College of Science, Technology and Medicine, 2002.
33. R.D. Moser, J. Kim and N.N. Mansour. Direct numerical simulation of turbulent channel flow up to Re_τ=590. *Phys. Fluids*, 11: 943-945, 1999.
34. B. Balakin, A.C. Hoffmann and P. Kosinski. The collision efficiency in a shear flow. *Chem. Eng. Sci.*, 68: 305-312, 2012.